Slow Protein Dynamics Elicits New Enzymatic Functions by Means of Epistatic Interactions

Maria-Agustina Rossi,[1] Timothy Palzkill,[2,3] Fabio C. L. Almeida,*[,4] and Alejandro J. Vila *[,1,5]

[1]Instituto de Biología Molecular y Celular de Rosario (IBR, CONICET-UNR), Ocampo and Esmeralda, Rosario, Argentina
[2]Department of Pharmacology and Chemical Biology, Baylor College of Medicine, Houston, USA
[3]Verna and Marrs McLean Department of Biochemistry and Molecular Biology, Baylor College of Medicine, Houston, USA
[4]Institute of Medical Biochemistry Leopoldo de Meis (IBqM) and National Center for Structural Biology and Bioimaging (CENABIO), Federal University of Rio de Janeiro (UFRJ), Rio de Janeiro, Brazil
[5]Facultad de Ciencias Bioquímicas y Farmacéuticas, Universidad Nacional de Rosario, Rosario, Argentina

***Corresponding authors:** E-mails: falmeida@bioqmed.ufrj.br; vila@ibr-conicet.gov.ar.

Associate editor: Julian Echave

Abstract

Protein evolution depends on the adaptation of these molecules to different functional challenges. This occurs by tuning their biochemical, biophysical, and structural traits through the accumulation of mutations. While the role of protein dynamics in biochemistry is well recognized, there are limited examples providing experimental evidence of the optimization of protein dynamics during evolution. Here we report an NMR study of four variants of the CTX-M β-lactamases, in which the interplay of two mutations outside the active site enhances the activity against a cephalosporin substrate, ceftazidime. The crystal structures of these enzymes do not account for this activity enhancement. By using NMR, here we show that the combination of these two mutations increases the backbone dynamics in a slow timescale and the exposure to the solvent of an otherwise buried β-sheet. The two mutations located in this β-sheet trigger conformational changes in loops located at the opposite side of the active site. We postulate that the most active variant explores alternative conformations that enable binding of the more challenging substrate ceftazidime. The impact of the mutations in the dynamics is context-dependent, in line with the epistatic effect observed in the catalytic activity of the different variants. These results reveal the existence of a dynamic network in CTX-M β-lactamases that has been exploited in evolution to provide a net gain-of-function, highlighting the role of alternative conformations in protein evolution.

Key words: **protein evolution, epistasis, β-lactamase, alternative conformations.**

Introduction

Protein dynamics are at the heart of protein function (Baldwin and Kay 2009; Smock and Gierasch 2009; Sekhar and Kay 2019; Kuzmanic et al. 2020). These dynamics encompass a wide range of frequencies that can match the timescales of different cellular and biochemical processes. The static pictures of proteins provided by X-ray crystallography provide snapshots of possible conformations, most likely representing the lowest-lying energy state under the conditions of the crystallization experiment. However, proteins can explore alternative, less populated conformations that can be functionally relevant (Bhabha et al. 2011; Clore 2014; Weikl and Paul 2014). Indeed, methodological advances in molecular dynamics and NMR spectroscopy have provided evidence of the existence of alternative conformations in equilibrium with the most populated one in solution, together with an assessment of the timescale of these processes (Korzhnev et al. 2004; Hansen and Kay 2014; Long et al. 2014). Knowledge of the less populated conformations enables shifting this equilibrium toward them by protein engineering eliciting new functions, as shown by a recent work (Knoverek et al. 2021). These equilibria are expected to play a key role in protein evolution, as shown in some studies (Tokuriki and Tawfik 2009; Zou et al. 2015; Campbell et al. 2016; Petrović et al. 2018). Nevertheless, a full picture of protein evolution including the concept of protein dynamics is still lacking.

The study of protein evolution is complicated by several issues: first, mutations have pleiotropic effects; second, the impact of mutations on a given trait is not always additive, giving rise to epistatic effects. In this regard, the impact of mutations in different biochemical and biophysical traits (function, stability) has been thoroughly studied in protein evolution (Petrović et al. 2018). In contrast, the study of protein dynamics as a molecular trait that can be fixed along an evolutionary pathway resulting in a gain-of-function has received limited attention (Tomatis et al. 2008; Gonzalez et al. 2016).

Antibiotic resistance mediated by β-lactamases is a unique model system to study protein evolution since bacterial survival in the presence of antibiotics depends on the

biophysical and functional features of a single enzyme. For this reason, some β-lactamases have been exploited as a model system to study protein evolution, such as the class A serine-β-lactamase (SBL) TEM (Weinreich et al. 2006; Salverda et al. 2010; Palzkill 2018; Gonzalez et al. 2019; Fantini et al. 2020; Cheng et al. 2021; Modi et al. 2021). The substrate profile of class A β-lactamases has been shaped by the evolutionary pressure of antibiotic use. SBLs with penicillinase activity (e.g., TEM and SHV families) are able to confer resistance against penicillins and first-generation cephalosporins. Some SBLs have evolved by gaining hydrolytic capacities against second- and third-generation cephalosporins. This is the case of the extended-spectrum serine-β-lactamases (ESBLs, such as those from the CTX-M family) (Bush 2018). The newer generations of antibiotics generally include larger chemical substituents that do not fit into the enzyme active sites. As a result, the expansion of the substrate spectrum of many SBLs results from mutations that enable the accommodation of these new drugs by augmenting the active-site volume (Salverda et al. 2010; Palzkill 2018). Ceftazidime, a third-generation cephalosporin, was originally developed based on this rationale. The bulky substituents in ceftazidime (in comparison to cefotaxime, fig. 1) make it a poor substrate that cannot fit into the deep and narrow active site of class A SBLs.

CTX-M β-lactamases are one of the most prevalent and widespread ESBLs among Gram-negative bacteria (Bonnet 2004; Doi et al. 2017; Bush and Bradford 2020; Castanheira et al. 2021). According to the β-lactamase database (Naas et al. 2017), 251 variants have been reported, with substitutions scattered throughout the protein structure (supplementary fig. S1A, Supplementary Material online). CTX-M β-lactamases possess a narrow and deep active site located between an α and an αβ domain, delimited by the β3 strand and several loops, known as 105-, SDN-, Ω-, and 240-loop (fig. 2 and supplementary fig. S1B, Supplementary Material online). CTX-M enzymes, in contrast to the family of TEM β-lactamases, are able to hydrolyze cefotaxime. However, they are less efficient in hydrolyzing ceftazidime. The Galán group proposed that ceftazidime and cefotaxime have been driving forces of the evolution of CTX-M variants (Novais et al. 2010). In particular, the D240G substitution has been identified as an initial mutation leading to different evolutionary pathways (Novais et al. 2010; Ghiglione et al. 2018).

CTX-M-14 has evolved ceftazidimase activity by only two substitutions, V231A and D240G at the two termini of the β3 strand (fig. 2), giving rise to CTX-M-16 (Bonnet et al. 2001). The single variants CTX-M-27 (D240G) (Bonnet et al. 2003) and CTX-M-9 (V231A) (Sabaté et al. 2000) are also present among clinical isolates (D'Andrea et al. 2013). However, the enhanced ceftazidimase activity is not accompanied by an enlargement of the active site (Chen et al. 2005), as reported for other class A β-lactamases (Poirel et al. 2002; Levitt et al. 2012; Patel et al. 2017; Palzkill 2018). The CTX-M-14, CTX-M-16, CTX-M-27, and CTX-M-9 crystal structures are almost identical in the unbound form (supplementary fig. S1C, Supplementary Material online) (Chen et al. 2005). An elegant analysis of the anisotropy factors in high-resolution crystal structures led Shoichet and coworkers to propose that the enhanced ceftazidimase activity could be related with a more flexible β3 strand (Chen et al. 2005). Molecular dynamics simulations have suggested that the D240G substitution would enable an open conformation favoring ceftazidime binding that is not captured by crystallography (Brown et al. 2020). However, there are several gaps to be understood to describe the adaptive success elicited by these mutations. On the one hand, there is a lack of direct experimental evidence accounting for these dynamics in solution. On the other hand, the structural bases of the gain-of-function induced by the hydrophobic mutation V231A are unknown, as is the epistatic interaction with mutation D240G.

Recent work from Bowman and coworkers (Porter et al. 2019) identified the presence of a binding pocket in CTX-M-9 that is created transiently by conformational fluctuations of the protein scaffold. This binding site (named a "cryptic pocket" by the authors) leads to the solvent exposure of otherwise buried protein residues through the displacement of the Ω-loop (Porter et al. 2019), a conserved region in SBLs that plays a key role in the evolution of hydrolytic abilities toward different cephalosporins (Banerjee et al. 1998; Palzkill 2018). Despite the fact that the Ω-loop sequence is not altered by these mutations (Chen et al. 2005), we reasoned that different conformations of the protein scaffold enabled by mutations at positions 231 and 240 could affect protein dynamics beyond the β3 strand structure, enlarging or increasing the population of a cryptic pocket, thus providing a mechanism to bind and hydrolyze ceftazidime. To address this issue, we studied the protein dynamics of these four CTX-M variants by NMR in a wide range of timescales, from picoseconds to hours. We found that CTX-M enzymes possess a rigid scaffold, as revealed by the fast backbone dynamics studies. This scaffold enables the accumulation of destabilizing mutations that enhance the catalytic activity against ceftazidime. Mutations V231A and D240G increase the slow dynamics in a slow timescale, with a large epistatic interaction that results in an overall increase in the dynamics of different active-site loops, including the Ω-loop, and also affects the positioning of catalytic residues, such as K73 and E166. We conclude that the interplay of these two mutations in CTX-M-16 increases the protein dynamics at the αβ domain, impacting the augmented exposure of buried protein regions in CTX-M-14. In other words, this reveals how evolution can tune the population of alternative conformations, resulting in improved fitness.

Results

The Two Mutations Show Positive Epistasis

All four CTX-M variants were purified with high yields (250 $mg_{CTX\text{-}M}/L_{culture}$). The double mutant (CTX-M-16)

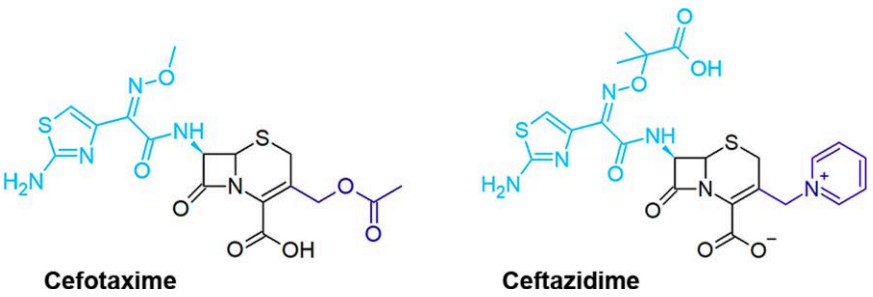

FIG. 1. Chemical structure of cefotaxime and ceftazidime. The R^1 (at the left) and the R^2 (at the right) chains are highlighted.

showed some precipitation at pH 8 or temperatures higher than 30 °C, in contrast to the high stability of the other three CTX-M enzymes under these conditions over long periods. We first replicated the kinetic analysis of the four CTX-M variants from refs (Chen et al. 2005; Patel et al. 2018) for cefotaxime, ceftazidime, and the first-generation cephalosporin cephalothin (fig. 3 and supplementary table S1, Supplementary Material online). The stability issues of CTX-M-16 did not compromise its kinetic characterization. Unfortunately, the high K_M values observed in all cases for ceftazidime hydrolysis precluded the determination of the individual kinetic parameters, as already discussed in the literature (Patel et al. 2018).

In line with previous reports, none of the mutations had a significant impact on the catalytic efficiency against cefotaxime and cephalothin, which are already good substrates of CTX-M-14 (fig. 3 and supplementary table S1, Supplementary Material online). The impact of these mutations is evident in the ceftazidimase activity, which is 15-fold increase in CTX-M-16 with respect to CTX-M-14. The single mutations had different effects on the activity against this substrate: mutation V231A (in CTX-M-9) did not induce significant changes in the kinetic parameters, while D240G (in CTX-M-27) increased the activity 5-fold. Figure 3 clearly shows a positive epistatic effect between these two mutations, since when V231A is added in the background of CTX-M-27, it results in a 3-fold increase in the ceftazidimase activity, in agreement with previous experiments (Chen et al. 2005).

Backbone Resonance Assignments

We recorded the ^{15}N-^{1}H HSQC spectrum of each CTX-M variant. The spectra of all variants showed an excellent cross-peak dispersion and intensity, notwithstanding the molecular mass of these proteins (28 kDa). Their signal dispersion revealed that all variants were properly folded (supplementary fig. S2, Supplementary Material online), allowing us to rule out the presence of unfolded or misfolded forms.

A comparison of the different spectra showed that those of CTX-M-14 and CTX-M-16 present the largest differences (supplementary fig. S3, Supplementary Material online). The backbone resonances of these two variants were assigned based on standard triple resonance experiments. Among the 251 nonproline residues of the CTX-M variants, 241 resonances were unambiguously assigned in CTX-M-14 (96%) and 244 (97%) in CTX-M-16 (supplementary tables S2 and S3, Supplementary Material online, respectively). The missing residues in both variants are M68 to T71, D163, I221, and S237. In addition, in CTX-M-14, residues L44 and active-site residues S72 and K73 remained unassigned. In contrast, S72 and K73 showed sharp resonances in CTX-M-16. Most of these residues are located near the active site or in solvent-exposed regions. The cross-peak of the catalytically essential S70 is also missing in the HSQC spectra of the class A SBLs Toho-1 (Sakhrani et al. 2021), TEM-1 (Savard and Gagné 2006), PSE-4 (Morin and Gagné 2009), and KPC-2 (VanPelt et al. 2019), suggesting that it is under conformational exchange. Finally, the H_N and N_H amide assignments from the CTX-M-14 spectrum were adapted to the HSQC of CTX-M-27 based on their high similarities (supplementary fig. S3 and table S4, Supplementary Material online), and those of CTX-M-16 were extrapolated to the chemical shifts of CTX-M-9 (supplementary fig. S3 and table S4, Supplementary Material online).

A secondary structure prediction using TALOS+ (Shen et al. 2009) was consistent with the crystal structures, revealing 11 α helices and 5 β strands (supplementary fig. S4, Supplementary Material online). Small differences were observed on residues 159–164 located in the Ω-loop. Their chemical shifts in CTX-M-14 are closer to those corresponding to a β strand, while in CTX-M-16, they display values attributable to a loop. Other small differences are located near the mutated sites.

The Point Mutations Induce Local Chemical Shift Perturbations

Substitutions D240G and V231A on CTX-M-14 elicited distinct chemical shift perturbations (CSPs) on the HSQC spectra (fig. 4 and supplementary fig. S5, Supplementary Material online). V231A perturbed 24 cross-peaks from residues located in the αβ domain, in particular resonances from residues located in strands β3 and β5, and in two loops: one connecting helix α9 and strand β3, and the loop connecting strands β4 and β5 (fig. 4). The D240G substitution induced small perturbations in 15 cross-peaks corresponding to residues from the 240- and 270-loops, and the resonances of T165-R178, located in the Ω-loop (fig. 4). Finally, the 45 perturbations in CTX-M-16

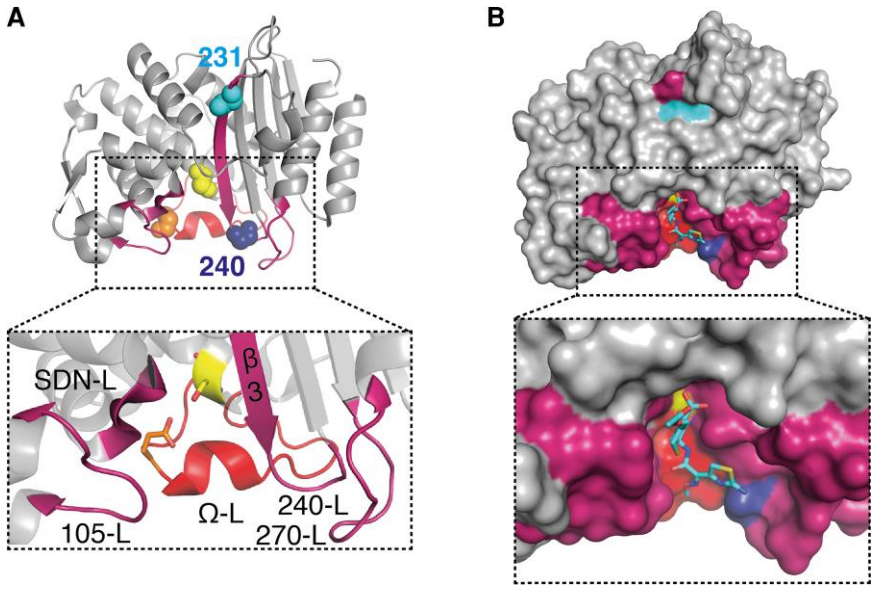

FIG. 2. CTX-M structure. (*A*) The Ω-loop (Ω-L), β3 strand, 105-loop (105-L), 240-loop (240-L), 270-loop (270-L) and SDN-loop (SDN-L) are highlighted. S70 (spheres or sticks, yellow), E166 (spheres or sticks, orange), and the substitution sites: V231A (spheres or sticks, cyan) and D240G (spheres or sticks, blue) are also shown (PDB 1ylt). (*B*) Surface representation of CTX-M enzymes. The color coding is the same used in (*A*) (PDB 4pm5).

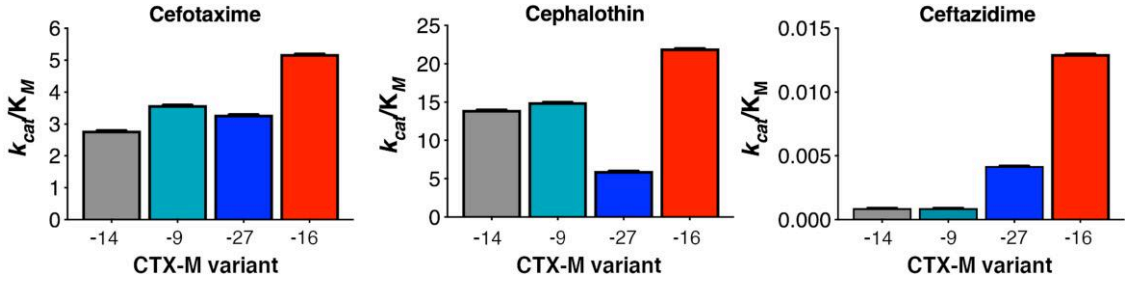

FIG. 3. Catalytic efficiencies for cephalosporins. k_{cat}/K_M for cefotaxime (left), cephalothin (middle), and ceftazidime (right) of CTX-M-14, CTX-M-9, CTX-M-27, and CTX-M-16. Units of k_{cat}/K_M are $\mu M^{-1} s^{-1}$.

correspond to the additive contributions of the two substitutions observed in the simple mutants (fig. 4).

Fast Backbone Dynamics Is Not Affected by the Mutations

To investigate the impact of substitutions V231A and D240G on the dynamics of the CTX-M-14 scaffold, longitudinal (R_1) and transverse (R_2) ^{15}N relaxation rates and $^{1}H-^{15}N$-NOE were measured. From these measurements, we calculated the S^2 parameter using the Lipari–Szabo formalism to obtain information on the backbone dynamics in the picosecond to nanosecond timescale (supplementary tables S5 and S6, Supplementary Material online).

The four β-lactamases displayed similar profiles (supplementary fig. S6, Supplementary Material online) and average relaxation parameters ($R_1 \sim 0.70\ s^{-1}$; $R_2 \sim 25\ s^{-1}$; $^{1}H-^{15}N$ NOE ~ 0.8; $S^2 \sim 0.9$; supplementary table S7, Supplementary Material online). The calculated correlation time of ~19.2 ns is consistent with a molecular weight of 28 kDa, allowing us to disregard the formation of dimeric species (supplementary table S7, Supplementary Material online). These data indicate that all variants are highly ordered and rigid, displaying few residues with low amplitude motions in the picosecond to nanosecond timescale.

Intermediate-range Dynamics Are Preserved Upon the Mutations

We next explored if the substitutions on CTX-M-14 impacted the dynamics in the microsecond to millisecond timescale. For this aim, the effective transverse relaxation rates ($R_{2,\ eff}$) were measured by means of CW-CPMG experiments. These experiments are challenging due to the molecular weight of CTX-M enzymes and the low-stability issues of CTX-M-16 that precluded recording spectra at temperatures higher than 25 °C and over long periods. Thus, CPMG experiments were performed on CTX-M-14 and CTX-M-16 at 20, 15, and 7 °C. Most residues displayed flat relaxation dispersion profiles, and only a few of them revealed the presence of fast-intermediate conformational exchange, that cannot be correlated to the introduced mutations (supplementary fig. S7, Supplementary Material online). In order to cover a wider range of timescales, we performed ^{15}N CEST experiments acquired at 7°C (data not shown). We did not observe significant

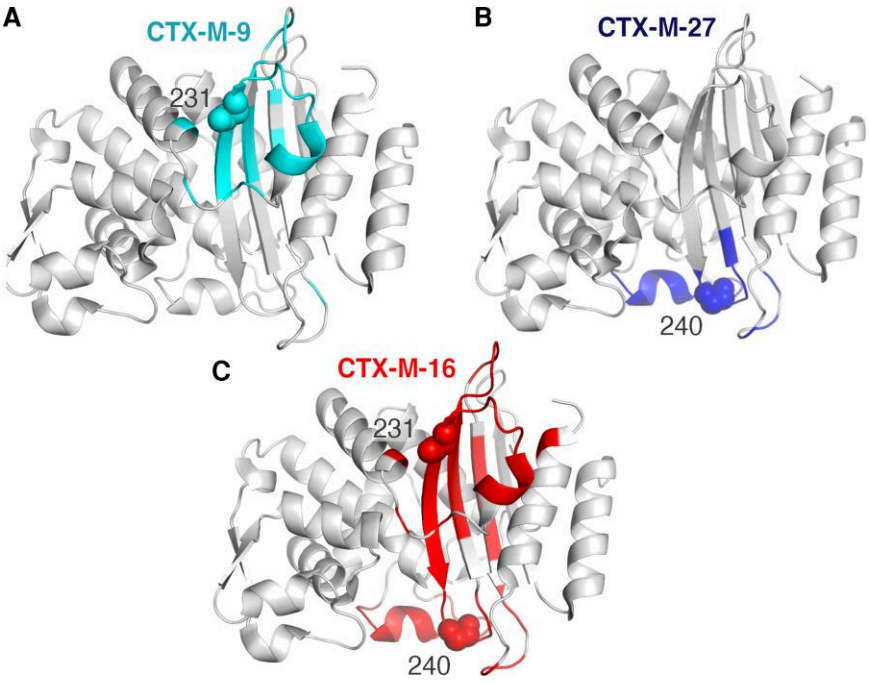

FIG. 4. Chemical shift perturbations. CSPs larger than 0.07 with respect to CTX-M-14 are mapped on the structures of CTX-M-9 (PDB 1ylj), CTX-M-27 (PDB 1ylp), and CTX-M-16 (PDB 1ylw).

dynamics within the CEST timescales (slow exchange regime). However, the poor signal-to-noise ratio of the CEST profiles for the low intense resonances (due to the size of the proteins) may preclude the detection of some dynamics, and CEST was uninformative for these residues. We can therefore discard the presence of relevant dynamics in the microsecond to millisecond timescale induced by these mutations.

Slow Dynamics Is Tuned by the Mutations in a Context-dependent Manner

Finally, we interrogated the protein dynamics in the millisecond to hour timescale by H/D exchange experiments (supplementary table S8, Supplementary Material online). We classified the H/D exchange regimes into three categories: fast (full exchange observed in <20 min), slow (exchange time between 20 min and 10 h), and no exchange (exchange times longer than 10 h). These results are summarized in figures 5, 6, and supplementary figure S8, Supplementary Material online.

In CTX-M-14, 36 residues showed fast exchange, all of them corresponding to solvent-exposed residues or residues located in loops (fig. 5 and supplementary fig. S8 and table S8, Supplementary Material online). Forty-nine residues exchanged in the slow regime, most of them located around the active site, on 105-loop, and in strand β3 (fig. 6 and supplementary fig. S8 and table S8, Supplementary Material online). None of the 129 residues located in the main α helixes and the β strands (except for β3) showed any exchange after 10 h (fig. 6 and supplementary fig. S8 and table S8, Supplementary Material online).

Both single mutants, CTX-M-9 and CTX-M-27, showed a significant increase in the number of signals under fast exchange compared with CTX-M-14, with 60 and 54 fast-exchanging residues, respectively (fig. 5 and supplementary fig. S8 and table S8, Supplementary Material online). On the other hand, these variants presented 46 (CTX-M-9) and 38 (CTX-M-27) residues in slow exchange (fig. 6 and supplementary fig. S8 and table S8, Supplementary Material online). In both cases, the mutations had a local effect, impacting on their immediate environment. The V231A substitution in CTX-M-9 impacted the exchange rates of six residues downstream from position 231 in the strand β3 and in the sequence stretch between the α9 helix and β3 strand, which connects the α and αβ domains (fig. 5). In the case of CTX-M-27, the D240G mutation showed faster exchange rates in the loop connecting α9 and β3, in a few residues at the C-terminus of the β3 strand, and in residues from the 270-loop (fig. 5).

The number of resonances with an enhanced exchange regime was significantly higher (103 residues) in the double mutant CTX-M-16 (fig. 5 and supplementary fig. S8 and table S8, Supplementary Material online). A simple inspection of the distribution of these residues in the protein structure reveals that the fast-exchanging residues in CTX-M-16 are much more than those expected based on a simple additive effect of the single mutants. All residues in the β3 strand spanning from positions 231 to 240, extending to the 240-loop and the N-terminus of the adjacent β4 strand were found to experience fast exchange. In addition, an increased exchange rate was detected in the different loops surrounding the active site: the 105-, SDN-, Ω-, and the 240-loop (fig. 5). Interestingly, the catalytic residue E166 was also in a fast exchange regime in CTX-M-16, in contrast with the lack of exchange in the other three variants (supplementary table S8, Supplementary Material online). Finally, 44

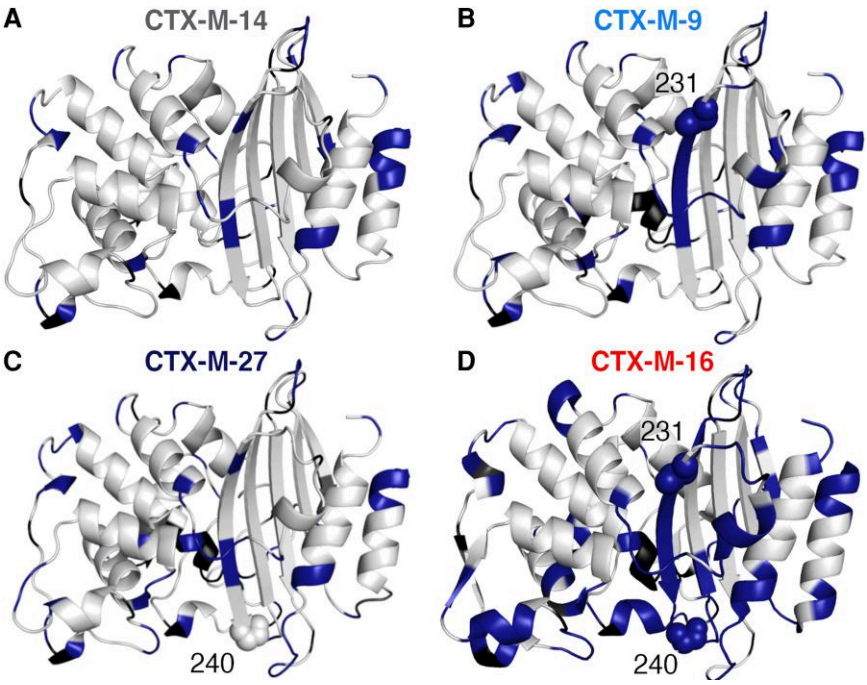

FIG. 5. Residues in H/D fast exchange regimen (<20 min) in (*A*) CTX-M-14 (PDBs 1ylt), (*B*) CTX-M-9 (PDB 1ylj), (*C*) CTX-M-27 (PDB 1ylp), and (*D*) CTX-M-16 (PDB 1ylw) are mapped in their crystal structure. Unassigned residues are indicated in black.

residues experienced a slow H/D exchange (fig. 6 and supplementary fig. S8 and table S8, Supplementary Material online), while 62 amide groups buried in the CTX-M structure do not exchange at all (fig. 6 and supplementary fig. S8 and table S8, Supplementary Material online).

In summary, the mutations at the termini of the β3 strand that expand the substrate spectrum of CTX-M enzymes strongly affected slow dynamics, and the extent of the impact of these mutations depends on the context, as observed for the ceftazidimase activity.

Discussion

In this work, we provide direct evidence of the role of protein dynamics in a slow exchange regime in one evolutionary pathway of the CTX-M β-lactamases that involves the substitution D240G, identified as a key step in the diversification of this family of enzymes (Novais et al. 2010).

By resorting to NMR spectroscopy, we have analyzed the dynamics on timescales ranging from picoseconds to hours of the parental enzyme CTX-M-14, the single mutants CTX-M-27 and CTX-M-9, and the double mutant CTX-M-16. Each substitution gave rise to CSPs on residues located mostly near each mutated site. The observed CSPs in the double mutant CTX-M-16 were additive (fig. 4 and supplementary fig. S5, Supplementary Material online), in contrast to the epistatic interaction between the two mutations observed in the catalytic efficiency. We therefore did not consider the CSPs for the analysis.

The scaffold of the CTX-M variants studied here is rigid, as revealed by the picosecond to nanosecond dynamics. The four variants showed limited dynamics, even at the Ω-loop (supplementary fig. S6, Supplementary Material online). These results and the calculated S^2 values are in agreement with similar NMR experiments in other class A β-lactamases such as Toho-1 (Sakhrani et al. 2021), TEM-1 (Savard and Gagné 2006), PSE-4 (Morin and Gagné 2009), and BlaC (Elings et al. 2020), and in chimeric variants inspired by TEM-1 and PSE-4 (Gobeil et al. 2019). Despite these β-lactamases sharing <40% of sequence identity and displaying different substrate profiles, the rigidity of the fold of class A β-lactamases seems to be conserved in enzymes that are currently undergoing different evolutionary strategies.

The key differences in dynamics were revealed by the H/D exchange experiments, which provide information regarding slow backbone dynamics (figs. 5, 6 and supplementary fig. S8, Supplementary Material online). Since these experiments are sampling a slow dynamic range, we restricted our analysis to the exchange phenomena detected at the first HSQC spectra (i.e., the shorter time frame detected by this experiment). The main impact of the mutations is located at the β3 strand (CTX-M-9) and in the 270-loop (CTX-M-27). NMR confirms that the introduction of Gly residues (such as in D240G) increases the dynamics of this strand. Ibuka and coworkers early suggested that the presence of several glycine residues in ESBLs confers flexibility to the β3 strand (Ibuka et al. 1999), which provides one of the active-site walls. The sequence of this strand in CTX-M-14 is $T_{230}VG_{232}DKTG_{236}SG_{238}D_{240}$. In this stretch, residue G236 is present in all class A β-lactamases, while G232 is present only in ESBLs (Ambler et al. 1991). Along these lines, Bonnet et al. (2003) suggested that the D240G mutation would further increase this flexibility. This hypothesis was supported by an analysis of high-resolution crystal structures of CTX-M-14, and the single mutants CTX-M-27 and

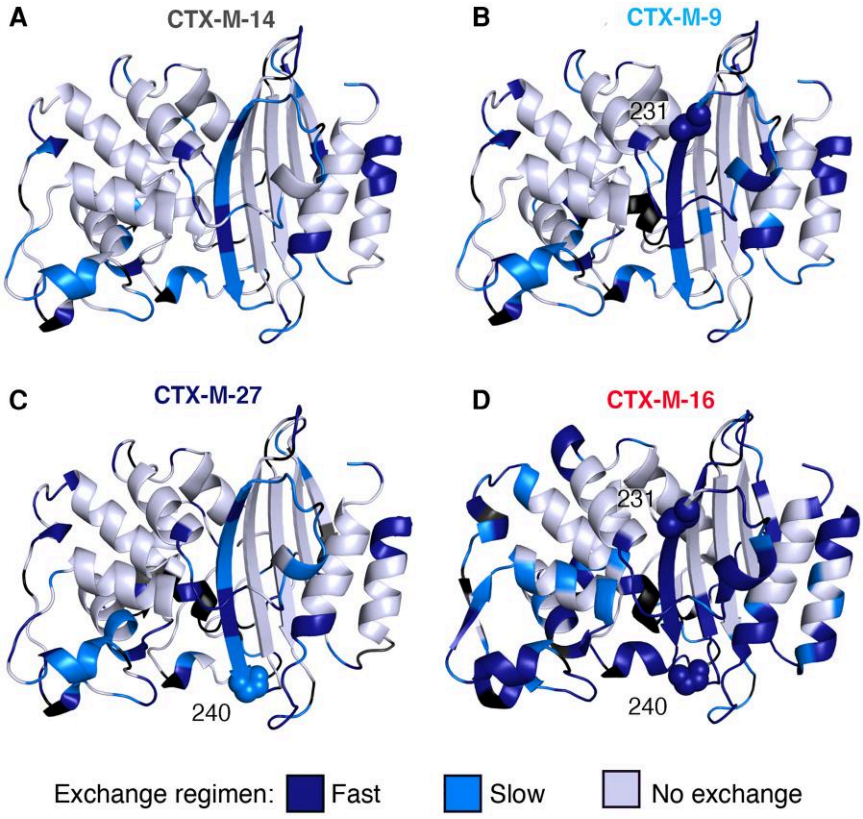

FIG. 6. Slow dynamics on CTX-M enzymes. Residues in fast, slow, and no exchange regimen in (*A*) CTX-M-14 (PDBs 1ylt), (*B*) CTX-M-9 (PDB 1ylj), (*C*) CTX-M-27 (PDB 1ylp), and (*D*) CTX-M-16 (PDB 1ylw) are mapped on to their crystal structure. Unassigned residues are indicated in black.

CTX-M-9 by Shoichet and coworkers. In this seminal work, changes in the thermal anisotropic parameters suggested a concerted movement of the β3 strand elicited by the D240G mutation (Chen et al. 2005). However, this analysis cannot explain the increase of ceftazidime hydrolysis in CTX-M-16 induced by the V231A substitution (fig. 3).

This NMR study provides several unexpected findings that help understanding the impact of these mutations in the gain of ceftazidimase activity. The V231A mutation alters the dynamics in protein regions that do not interact directly with the substrate, in contrast to D240G. This accounts for the lack of improvement of activity against ceftazidime in CTX-M-9 versus CTX-M-27 (fig. 3). Only the combination of the two mutations results in increased dynamics of the entire β3 strand. In this regard, when mutation V231A is added after D240G to give rise to CTX-M-16, it results in a much larger enhancement of the exchange rates, revealing that the epistatic effect observed in the catalytic activity is due to the synergistic interaction between these mutations reflected in the backbone dynamics.

Many other residues show altered dynamics only in the double mutant, that is, the epistatic interaction is not limited to effects in the strand β3. First, residue E166, acting as a general base in the catalytic mechanism (Banerjee et al. 1998; Palzkill 2018; Tooke et al. 2019), only showed fast H/D exchange in the double mutant CTX-M-16. Studies on different SBLs have shown that the conformation of E166 is tuned by different active-site mutations (Banerjee et al. 1998; Palzkill 2018; Brown et al. 2020; Tooke et al. 2021). Mutations in position 240 are responsible for this effect when combined with other substitutions mostly located in the active-site loops (supplementary fig. S9, Supplementary Material online, cf. in CTX-M-27, KPC-2, and KPC-4) (Brown et al. 2020; Tooke et al. 2021). We propose that changes in the β3 strand induced by the synergistic interaction of the substitutions in positions 231 and 240 result in an orientation of E166 favoring ceftazidime hydrolysis.

Second, the signal corresponding to residue K73 could not be assigned in CTX-M-14, 9, and 27. This residue is involved in the acylation step and makes hydrogen bonding interactions with the catalytic S70 and key water molecules in the active site (Nichols et al. 2015; Palzkill 2018; Tooke et al. 2019; Pemberton et al. 2020). The absence of this resonance can be accounted for by assuming that K73 is undergoing dynamics in an intermediate timescale, in agreement with the two conformations reported in the crystal structures of CTX-M-9 and CTX-M-14. In the double-mutant CTX-M-16, K73 was observed as a single, sharp line, revealing that its dynamics is modified when the two mutations are present. This can be interpreted by assuming that: (1) K73 is adopting a single conformation, more favorable for ceftazidime hydrolysis or (2) K73 is under a more rapid exchange between two conformations, lowering the energetic barrier to access the conformation favoring ceftazidime hydrolysis.

Third, CTX-M-16 also exhibited increased dynamics in the active-site loops: 105-, SDN-, 240-, 270-, and Ω-loop. Fourth, we observed increased dynamics in the loop connecting helix α9 and strand β3 that links the α and the αβ domains. In summary, the slow dynamics elicited by the two mutations in the

β3 strand is transmitted to essential active site residues (E166 and K73) and all active-site loops.

We interpret that this effect is due to a breathing mechanism of the enzyme that partially exposes the β3 strand to the solvent, as revealed by the H/D exchange rates in the double mutant. This agrees with the tradeoff between activity and stability proposed by Shoichet (Chen et al. 2005) and Palzkill (Patel et al. 2015, 2018; Brown et al. 2020), who showed that these substitutions decrease the thermodynamic stability. We propose that the reduced stability of the double variant in solution is due to this breathing mechanism that transiently exposes hydrophobic regions (supplementary fig. S10, Supplementary Material online), leading to partial precipitation. This can be directly attributed to the increased dynamics in the loop connecting the α and αβ domains that may lead transiently to a more open active site that can better recognize ceftazidime. Although it is tempting to speculate that this may be due to a larger population containing the cryptic pocket identified in CTX-M-9 (Porter et al. 2019), our results do not provide a direct link with the findings from the Bowman group, which may correspond to a different timescale, but do support the concept of a functional role for the cryptic sites. Despite the sampled timescale observed may be considered slow, the nonadditivity of this effect correlates with the epistatic interaction between the mutations that results in an enhanced activity against ceftazidime. In the case of Metallo-β-lactamases, loop dynamics in a faster timescale [revealed by relaxation dispersion experiments (González et al. 2016)] was correlated with an expansion of the substrate profile. However, an increase in loop dynamics is less challenging for the protein fold than the breathing mechanism herein proposed, and a slower timescale is consistent with this mechanism.

A rational redesign of the β-lactamase TEM aimed at increasing the population of a cryptic site led to an increase in the penicillinase activity of this protein, compromising the activity against cefotaxime (Knoverek et al. 2021). This activity tradeoff between penicillin and cefotaxime hydrolysis has been linked to the population of the cryptic site of TEM enzymes (Hart et al. 2016). This tradeoff has not been reported for CTX-M β-lactamases (Bonnet 2004; Palzkill 2018), suggesting that similar folds may have different cryptic sites, a hypothesis that deserves further analysis.

Our current results uncover the presence of a dynamic network in the CTX-M fold that is exploited in evolution by augmenting the backbone dynamics based on a few key mutations, even far from the active site. This contrasts with the dynamic studies of other SBLs such as TEM, PSE (Gobeil et al. 2019), and KPC variants (Galdadas et al. 2021). Epistatic interactions in the metallo-β-lactamase BcII occurred by changes in the hydrogen bonding interactions of second sphere residues that increased the dynamics of the active-site loops in the microsecond to millisecond timescale (González et al. 2016). In this case, we observe a subtle change in a buried β strand that is transmitted to the whole protein structure and is operative in a slower timescale. Overall, these results highlight the relevance of epistatic interactions in protein evolution and their direct link with protein dynamics. Finally, this study strongly supports the role of alternative conformations and cryptic pockets in protein evolution.

Materials and Methods

Numbering Scheme

Residues are numbered according to the SBLs standard numbering scheme (Ambler et al. 1991).

Bacterial Strains and Plasmids

Escherichia coli DH5α was used for cloning and *E. coli* BL21(DE3) for protein expression and purification. CTX-M (residues 25–290) genes were inserted into the pET28b$^+$(TEV) plasmid (with the TEV cleavage site instead of thrombin) (Kapust et al. 2001; Houben et al. 2007) and the resulting plasmids were used for protein expression.

Site-directed Mutagenesis

All CTX-M variants were constructed by site-directed mutagenesis. The primers, (Genbiotech, Argentina) listed in supplementary table S9, Supplementary Material online, were used to introduce the desired mutations into the pTP123-CTXM14 (Patel et al. 2015) plasmid using Pfx Platinum DNA polymerase (Invitrogen, USA). All constructs were verified by DNA sequencing (University of Maine DNA Sequencing Facility, USA). Then, the coding regions for residues 25–290 (no signal peptide) were PCR-amplified with Taq polymerase (Invitrogen, USA) and the primers (Genbiotech, Argentina) listed in supplementary table S9, Supplementary Material online. The amplicons were digested with NdeI and XhoI (Invitrogen, USA) and ligated in the pET28b$^+$(TEV) plasmid, that had been digested with the same enzymes. The gene sequences were verified with DNA sequencing.

Protein Expression and Purification

Escherichia coli BL21(DE3) cells were transformed with the different expression plasmids [pET28b$^+$(TEV)-CTX-M-14, -9, -27, or -16]. They were then inoculated in minimal medium M9 supplemented with 50 μg/ml kanamycin and were grown to $OD_{600nm} \sim 0.6$. For the NMR experiments, the medium was supplemented with the isotopes: ^{13}C and/or ^{15}N (Cambridge Isotope Laboratories, USA). Protein expression was induced with 200 μM IPTG and the cultures were incubated overnight at 20°C under gentle agitation. The cells were collected by centrifugation and disrupted by sonication in buffer A (50 mM Tris–HCl pH 8, 200 mM NaCl) supplemented with 10 μg/ml DNAse, 4 mM $MgCl_2$, and 2 mM PMSF. The insoluble fractions were removed by centrifugation. The crude extracts were loaded in Ni-sepharose columns equilibrated with Buffer A and then washed with Buffer A supplemented with 4% imidazole. The fused proteins were eluted with a linear gradient (100 ml, Buffer A supplemented with 4–100% 500 mM imidazole). His_6-CTX-M-14, −9, or −27 were

dialyzed against Buffer A for 16 h to eliminate the imidazole. His_6-CTX-M-16 was loaded in a desalting column (Sephadex G-25 Fine resin) equilibrated with 50 mM Tris–HCl pH 7.5, 200 mM NaCl, and stored overnight. The His_6-tags of all CTX-M enzymes were cleaved with TEV protease (1:75 TEV:His_6-CTX-M) for 2 h at 25°C. CTX-M-16 was then loaded in a desalting column equilibrated with Buffer A. To separate the cleaved His_6-tags from the β-lactamases, the samples were loaded again in Ni-Sepharose columns and CTX-M enzymes were collected in the flow-through with a purity >95%, as determined by SDS–PAGE. The concentration of the protein samples was determined from the absorbance at 280 nm using a molar absorption coefficient (ϵ_{280}) of 24,000 M^{-1} c/m. The four variants were purified with a similar average yield of 250 $mg_{CTX\text{-}M}/L_{culture}$ and the expected molecular weight of 28 kDa.

Enzyme Kinetics

The steady-state Michaelis–Menten kinetic parameters were determined to follow β-lactam antibiotic hydrolysis by CTX-M enzymes using a Jasco V-670 spectrophotometer. The substrates were monitored at 260 nm with the following molar absorption coefficient: cefotaxime $\Delta\epsilon_{262} = -7250\ M^{-1}$ c/m, ceftazidime, $\Delta\varepsilon_{256} = -7600\ M^{-1}$ c/m, and cephalothin $\Delta\epsilon_{262} = -7660\ M^{-1}$ c/m. The CTX-M concentration used was dependent on the enzyme:substrate pair: 2 nM (CTX-M-14, -9, -27, and -16 and cefotaxime), 1 nM (CTX-M-14, -9, -27, and -16 and cephalothin), 1 μM (CTX-M-14 and CTX-M-9 and ceftazidime), 300 nM (CTX-M-27 and ceftazidime), and 40 nM (CTX-M-16 and ceftazidime). Reactions were performed in 50 mM sodium phosphate pH 7.0 and 0.1 mg/ml BSA. Initial velocity reaction rates were obtained for different substrate concentrations and fitted using GraphPad Prism 5 to obtain the steady-state parameters. Ceftazidime hydrolysis could not be saturated by measurable concentrations due to the high K_m, so the second-order rate constant at steady-state, k_{cat}/K_m, was determined by fitting the progress curves to the equation $v = k_{cat}/K_m[E][S]$.

NMR Samples, Data Acquisition and Processing

All experiments were acquired with TopSpin 3.5 (Bruker) and standard techniques. The buffer was 100 mM MES pH 6.4, 200 mM NaCl, and 10% D_2O. All the programs were provided by the NMRbox platform (Maciejewski et al. 2017).

Backbone Resonance Assignment

The C_α, C_β, C_O, H_N, and N_H chemical shifts for CTX-M-14 and CTX-M-16 were assigned using the following experiments: $^1H–^{15}N$ HSQC and the three-dimensional spectra: HNCA, HN(CO)CA, HNCO, HN(CA)CO, CBCA(CO)NH, and HNCACB (Gardner and Kay 1998). The spectra were acquired at 20 °C on 1 mM samples at a magnetic field of 700 MHz [Bruker Avance III spectrometer equipped with a triple resonance inverse (TXI) probehead]. All spectra were analyzed with CARA (Keller 2004). The CTX-M secondary structure was predicted with TALOS+ (Shen et al. 2009) and the chemical shift perturbations (CSPs) for ^{15}N-^1H resonances were calculated [$CSP_{NH} = (\Delta\delta_H^2 + (\Delta\delta_N/5)^2)^{1/2}$].

Relaxation Experiments in Picosecond–Nanosecond TimeScale

In proteins, the fast dynamic motions arise in the picosecond to nanosecond timescale. A complete set of experiments was measured with 700 μM samples of CTX-M-14, -9, -27, and -16. It includes inversion recovery experiments (for R_1 determination rates), Carr–Purcell–Meiboom–Gill (CPMG) (for R_2 determination rates), and the $^1H–^{15}N$ nuclear overhauser effects (NOE) using standard pulse schemes. All experiments were carried out at 20 °C and 700 MHz (Bruker Avance III Spectrometer equipped with a triple resonance inverse [TXI] probe head) and were acquired in an interleaved 3D experiment. The Data Analysis routine of CCPN (Vranken et al. 2005) was used for the analysis. For R_1 determination, the relaxation delays for inversion recovery were: 100, 200, 400, 600, 800, 1000, 1300, 1600, and 2000 ms with a recycling delay of 3 s. For R_2 measurements, the CPMG delays were: 16.96, 33.92, 50.88, 67.84, 84.80, 101.76, 118.72, and 135.68 ms with a recycling delay of 3 s. For $^1H–^{15}N$ NOE experiments, the recycling delay was 5 s.

The relaxation data of the four enzymes were analyzed using the model-free approach introduced by Lipari and Szabo (1982a, 1982b). It provides information about the global tumbling, characterized by the global correlation time (τ_c), and local motions that are described by the order parameter (S^2). Tensor 2.0 (Dosset et al. 2000) software was used with an anisotropic diffusion model and the following PDB files: CTX-M-14: 1ylt, CTX-M-9: 1ylt, CTX-M-27: 1ylt, and CTX-M-16:1ylw.

Relaxation Dispersion Experiments

^{15}N CPMG relaxation dispersion experiments were acquired on 1 mM samples of CTX-M-14 and CTX-M-16 at 7, 15, and 20 °C and 600 and 800 MHz using a decoupling continuous wave (CW) during the CPMG pulse train (Hansen et al. 2008). A constant relaxation time (T_{relax}) of 30 ms and a CPMG frequency (ν_{CPMG}) = $1/(2\tau)$ between 25 and 1000 Hz were used, where τ is the separation time of two consecutive 180° refocusing pulses of the ^{15}N CPMG pulse train. Spectra were transformed using the NMRpipe (Delaglio et al. 1995) program.

The relaxation dispersion profiles [$R_{2,\ eff}$ (ν_{CPMG})] were calculated from the intensity of the peaks (I) in a series of $^1H–^{15}N$ correlation spectra at different ν_{CPMG}. The intensities were adjusted to the equation: $R_{2,\ eff}(\nu_{CPMG}) = -1/T_{relax}\ln(I/I_0)$, where the intensity of the signal (I) and (I_0) corresponds to the spectrum using a T_{relax} of 30 and 0 ms, respectively.

CEST Experiments

CEST experiments (Vallurupalli et al. 2012) were performed with CTX-M-14 and CTX-M-16 on 1 mM samples

at 7 °C and 21.1 T. The acquired data comprised a series of 2D spectra with ^{15}N offsets ranging between 98.0 and 136.5 ppm obtained in increments of 0.5 ppm. The saturation B1 field was 25 Hz with an exchange time of 400 ms. The HSQC spectra were acquired with 1024 × 150 complex points (t1, t2) and a relaxation delay between scans of 1.55 s. We used a 3.67 kHz ^{1}H decoupling field.

Proton–Deuterium Amide Exchange

CTX-M samples at 700 µM were lyophilized and then dissolved in 99.8% D_2O (Cambridge Isotope Laboratories, USA). Then, a series of ^{1}H–^{15}N HSQC spectra were acquired in tandem for 48 h at 700 MHz. The disappearance of each cross-peak due to the proton/deuterium exchange was analyzed by quantitating the intensity in spectra recorded at 20, 40, 60 min, 5, 7.5, 10, 15, 20, 25, 30, and 40 h. The exchange rates were classified into three categories: fast (<20 min), slow (between 40 min and 10 h), and no exchange (>10 h).

Supplementary Material

Supplementary data are available at *Molecular Biology and Evolution* online.

Acknowledgments

This work was supported by grant 2R01AI100560-06A1 (NIAID) and PICT-2016-1657 (FONCyT) to A.J.V., grant NIH AI32956 to T.P., grants 255.940/2020, 239.229/2018, 210.361/2015 and 204.432/2014 (FAPERJ), and 309564/2017 (CNPq) to F.C.L.A. This study made use of NMRbox: National Center for Biomolecular NMR Data Processing and Analysis, a Biomedical Technology Research Resource (BTRR), which is supported by NIH grant P41GM111135 (NIGMS). A. J. V. is a staff member from CONICET . M.-A.R. was the recipient of a doctoral fellowship from CONICET.

Data Availability

All data are available from the authors on request.

References

Ambler RP, Coulson AFW, Frère JM, Ghuysen JM, Joris B, Forsman M, Levesque RC, Tiraby G, Waley SG. 1991. A standard numbering scheme for the class A beta-lactamases. *Biochem J*. **276**:269–270.

Baldwin AJ, Kay LE. 2009. NMR spectroscopy brings invisible protein states into focus. *Nat Chem Biol*. **5**:808–814.

Banerjee S, Pieper U, Kapadia G, Pannell LK, Herzberg O. 1998. Role of the Ω-loop in the activity, substrate specificity, and structure of class A β-lactamase. *Biochemistry* **37**:3286–3296.

Bhabha G, Lee J, Ekiert DC, Gam J, Wilson IA, Dyson HJ, Benkovic SJ, Wright PE. 2011. A dynamic knockout reveals that conformational fluctuations influence the chemical step of enzyme catalysis. *Science* **332**:234–238.

Bonnet R. 2004. Growing group of extended-spectrum beta-lactamases: the CTX-M enzymes. *Antimicrob Agents Chemother* **48**:1–14.

Bonnet R, Dutour C, Sampaio JLM, Chanal C, Sirot D, Labia R, De Champs C, Sirot J. 2001. Novel cefotaximase (CTX-M-16) with increased catalytic efficiency due to substitution Asp-240-Gly. *Antimicrob Agents Chemother*. **45**:2269–2275.

Bonnet R, Recule C, Baraduc R, Chanal C, Sirot D, De Champs C, Sirot J. 2003. Effect of D240G substitution in a novel ESBL CTX-M-27. *J Antimicrob Chemother*. **52**:29–35.

Brown CA, Hu L, Sun Z, Patel MP, Singh S, Porter JR, Sankaran B, Prasad BVV, Bowman GR, Palzkill T. 2020. Antagonism between substitutions in B-lactamase explains a path not taken in the evolution of bacterial drug resistance. *J Biol Chem*. **295**:7376–7390.

Bush K. 2018. Past and present perspectives on β-lactamases. *Antimicrob Agents Chemother*. **62**:e01076-18.

Bush K, Bradford PA. 2020. Epidemiology of β-lactamase-producing pathogens. *Clin Microbiol Rev*. **33**:e00047-19.

Campbell E, Kaltenbach M, Correy GJ, Carr PD, Porebski BT, Livingstone EK, Afriat-Jurnou L, Buckle AM, Weik M, Hollfelder F, *et al.* 2016. The role of protein dynamics in the evolution of new enzyme function. *Nat Chem Biol*. **12**:944–950.

Castanheira M, Simner PJ, Bradford PA. 2021. Extended-spectrum β-lactamases: an update on their characteristics, epidemiology and detection. *JAC-Antimicrob Resist*. **3**:dlab092.

Chen Y, Delmas J, Sirot J, Shoichet B, Bonnet R. 2005. Atomic resolution structures of CTX-M β-lactamases: extended spectrum activities from increased mobility and decreased stability. *J Mol Biol*. **348**:349–362.

Cheng Q, Cheung YC, Chan EWC, Wong KY, Chen S. 2021. Unveiling the evolution routes of TEM-type extended-spectrum β-lactamases. *Int J Antimicrob Agents*. **59**:106498.

Clore GM. 2014. Interplay between conformational selection and induced fit in multidomain protein–ligand binding probed by paramagnetic relaxation enhancement. *Biophys Chem*. **186**:3–12.

D'Andrea MM, Arena F, Pallecchi L, Rossolini GM. 2013. CTX-M-type β-lactamases: a successful story of antibiotic resistance. *Int J Med Microbiol*. **303**:305–317.

Delaglio F, Grzesiek S, GeertenW V, Zhu G, Pfeifer J, Bax A. 1995. NMRPipe: a multidimensional spectral processing system based on UNIX pipes. *J Biomol NMR*. **6**:277–293.

Doi Y, Iovleva A, Bonomo RA. 2017. The ecology of extended-spectrum β-lactamases (ESBLs) in the developed world. *J Travel Med*. **24**:S44–S51.

Dosset P, Hus J-C, Blackledge M, Marion D. 2000. Efficient analysis of macromolecular rotational diffusion from heteronuclear relaxation data. *J Biomol NMR*. **16**:23–28.

Elings W, Gaur A, Blok AJ, Timmer M, van Ingen H, Ubbink M. 2020. β-Lactamase of *Mycobacterium tuberculosis* shows dynamics in the active site that increase upon inhibitor binding. *Antimicrob Agents Chemother*. **64**:e02025-19.

Fantini M, Lisi S, De Los Rios P, Cattaneo A, Pastore A. 2020. Protein structural information and evolutionary landscape by in vitro evolution. *Mol Biol Evol*. **37**:1179–1192.

Galdadas I, Qu S, Oliveira ASF, Olehnovics E, Mack AR, Mojica MF, Agarwal PK, Tooke CL, Gervasio FL, Spencer J, *et al.* 2021. Allosteric communication in class A β-lactamases occurs via cooperative coupling of loop dynamics. *eLife* **10**:e66567.

Gardner KH, Kay LE. 1998. The use of ^{2}H, ^{13}C, ^{15}N multidimensional NMR to study structure and dynamics of proteins. *Annu Rev Biophys Biomol Struct*. **27**:357–406.

Ghiglione B, Rodríguez MM, Curto L, Brunetti F, Dropa M, Bonomo RA, Power P, Gutkind G. 2018. Defining substrate specificity in the CTX-M family: the role of Asp240 in ceftazidime hydrolysis. *Antimicrob Agents Chemother*. **62**:e00116-18.

Gobeil SMC, Ebert MCJC, Park J, Gagné D, Doucet N, Berghuis AM, Pleiss J, Pelletier JN. 2019. The structural dynamics of engineered β-lactamases vary broadly on three timescales yet sustain native function. *Sci Rep*. **9**:6656.

Gonzalez MM, Abriata LA, Tomatis PE, Vila AJ. 2016. Optimization of conformational dynamics in an epistatic evolutionary trajectory. *Mol Biol Evol*. **33**:1768–1776.

Gonzalez CE, Roberts P, Ostermeier M. 2019. Fitness effects of single amino acid insertions and deletions in TEM-1 β-lactamase. *J Mol Biol*. **431**:2320–2330.

Hansen AL, Kay LE. 2014. Measurement of histidine pK_a values and tautomer populations in invisible protein states. *Proc Natl Acad Sci U S A*. **111**:e1705–12.

Hansen DF, Vallurupalli P, Kay LE. 2008. An improved 15N relaxation dispersion experiment for the measurement of millisecond time-scale dynamics in proteins. *J Phys Chem B*. **112**:5898–5904.

Hart KM, Ho CMW, Dutta S, Gross ML, Bowman GR. 2016. Modelling proteins' hidden conformations to predict antibiotic resistance. *Nat Commun*. **7**:12965.

Houben K, Marion D, Tarbouriech N, Ruigrok RW, Blanchard L. 2007. Interaction of the C-terminal domains of sendai virus N and P proteins: comparison of polymerase-nucleocapsid interactions within the paramyxovirus family. *J Virol*. **81**:6807–6816.

Ibuka A, Taguchi A, Ishiguro M, Fushinobu S, Ishii Y, Kamitori S, Okuyama K, Yamaguchi K, Konno M, Matsuzawa H. 1999. Crystal structure of the E166A mutant of extended-spectrum β-lactamase toho-1 at 1.8 Å resolution. *J Mol Biol*. **285**: 2079–2087.

Kapust RB, Tozser J, Fox JD, Anderson DE, Cherry S, Copeland TD, Waugh DS. 2001. Tobacco etch virus protease: mechanism of autolysis and rational design of stable mutants with wild-type catalytic proficiency. *Protein Eng*. **14**:993–1000.

Keller R. 2004. *The computer aided resonance assignment tutorial*. Goldau: Cantina Verl.

Knoverek CR, Mallimadugula UL, Singh S, Rennella E, Frederick TE, Yuwen T, Raavicharla S, Kay LE, Bowman GR. 2021. Opening of a cryptic pocket in β-lactamase increases penicillinase activity. *Proc Natl Acad Sci U S A*. **118**:e2106473118.

Korzhnev DM, Salvatella X, Vendruscolo M, Di Nardo AA, Davidson AR, Dobson CM, Kay LE. 2004. Low-populated folding intermediates of Fyn SH3 characterized by relaxation dispersion NMR. *Nature* **430**:586–590.

Kuzmanic A, Bowman GR, Juarez-Jimenez J, Michel J, Gervasio FL. 2020. Investigating cryptic binding sites by molecular dynamics simulations. *Acc Chem Res*. **53**:654–661.

Levitt PS, Papp-Wallace KM, Taracila MA, Hujer AM, Winkler ML, Smith KM, Xu Y, Harris ME, Bonomo RA. 2012. Exploring the role of a conserved class A residue in the Ω-loop of KPC-2 β-lactamase: a mechanism for ceftazidime hydrolysis. *J Biol Chem*. **287**:31783–31793.

Lipari G, Szabo A. 1982a. Model-free approach to the interpretation of nuclear magnetic resonance relaxation in macromolecules. 2. Analysis of experimental results. *J Am Chem Soc*. **104**:4559–4570.

Lipari G, Szabo A. 1982b. Model-free approach to the interpretation of nuclear magnetic resonance relaxation in macromolecules. 1. Theory and range of validity. *J Am Chem Soc*. **104**:4546–4559.

Long D, Bouvignies G, Kay LE. 2014. Measuring hydrogen exchange rates in invisible protein excited states. *Proc Natl Acad Sci U S A*. **111**:8820–8825.

Maciejewski MW, Schuyler AD, Gryk MR, Moraru II, Romero PR, Ulrich EL, Eghbalnia HR, Livny M, Delaglio F, Hoch JC. 2017. NMRbox: a resource for biomolecular NMR computation. *Biophys J*. **112**:1529–1534.

Modi T, Risso VA, Martinez-Rodriguez S, Gavira JA, Mebrat MD, Van Horn WD, Sanchez-Ruiz JM, Banu Ozkan S. 2021. Hinge-shift mechanism as a protein design principle for the evolution of β-lactamases from substrate promiscuity to specificity. *Nat Commun*. **12**:1852.

Morin S, Gagné SM. 2009. NMR dynamics of PSE-4 β-lactamase: an interplay of ps-ns order and μs-ms motions in the active site. *Biophys J*. **96**:4681–4691.

Naas T, Oueslati S, Bonnin RA, Dabos ML, Zavala A, Dortet L, Retailleau P, Iorga BI. 2017. Beta-lactamase database (BLDB)–structure and function. *J Enzyme Inhib Med Chem*. **32**: 917–919.

Nichols DA, Hargis JC, Sanishvili R, Jaishankar P, Defrees K, Smith EW, Wang KK, Prati F, Renslo AR, Woodcock HL, *et al*. 2015. Ligand-induced proton transfer and low-barrier hydrogen bond revealed by X-ray crystallography. *J Am Chem Soc*. **137**:8086–8095.

Novais Â, Comas I, Baquero F, Cantón R, Coque TM, Moya A, González-Candelas F, Galán J-C. 2010. Evolutionary trajectories of beta-lactamase CTX-M-1 cluster enzymes: predicting antibiotic resistance. *PLoS Pathog*. **6**:e1000735.

Palzkill T. 2018. Structural and mechanistic basis for extended-spectrum drug-resistance mutations in altering the specificity of TEM, CTX-M, and KPC β-lactamases. *Front Mol Biosci*. **5**:1–19.

Patel MP, Fryszczyn BG, Palzkill T. 2015. Characterization of the global stabilizing substitution A77V and its role in the evolution of CTX-M β-lactamases. *Antimicrob Agents Chemother*. **59**:6741–6748.

Patel MP, Hu L, Brown CA, Sun Z, Adamski CJ, Stojanoski V, Sankaran B, Prasad BVV, Palzkill T. 2018. Synergistic effects of functionally distinct substitutions in β-lactamase variants shed light on the evolution of bacterial drug resistance. *J Biol Chem*. **293**: 17971–17984.

Patel MP, Hu L, Stojanoski V, Sankaran B, Prasad BVV, Palzkill T. 2017. The drug-resistant variant P167S expands the substrate profile of CTX-M β-lactamases for oxyimino-cephalosporin antibiotics by enlarging the active site upon acylation. *Biochemistry* **56**: 3443–3453.

Pemberton OA, Noor RE, Kumar MVV, Sanishvili R, Kemp MT, Kearns FL, Woodcock HL, Gelis I, Chen Y. 2020. Mechanism of proton transfer in class A β-lactamase catalysis and inhibition by avibactam. *Proc Natl Acad Sci U S A*. **117**:5818–5825.

Petrović D, Risso VA, Kamerlin SCL, Sanchez-Ruiz JM. 2018. Conformational dynamics and enzyme evolution. *J R Soc Interface*. **15**:20180330.

Poirel L, Gniadkowski M, Nordmann P. 2002. Biochemical analysis of the ceftazidime-hydrolysing extended-spectrum β-lactamase CTX-M-15 and of its structurally related β-lactamase CTX-M-3. *J Antimicrob Chemother*. **50**:1031–1034.

Porter JR, Moeder KE, Sibbald CA, Zimmerman MI, Hart KM, Greenberg MJ, Bowman GR. 2019. Cooperative changes in solvent exposure identify cryptic pockets, switches, and allosteric coupling. *Biophys J*. **116**:818–830.

Sabaté M, Tarragó R, Navarro F, Miró E, Vergés C, Barbé J, Prats G. 2000. Cloning and sequence of the gene encoding a novel cefotaxime-hydrolyzing beta-lactamase (CTX-M-9) from *Escherichia coli* in Spain. *Antimicrob Agents Chemother*. **44**: 1970–1973.

Sakhrani VV, Ghosh RK, Hilario E, Weiss KL, Coates L, Mueller LJ. 2021. Toho-1 β-lactamase: backbone chemical shift assignments and changes in dynamics upon binding with avibactam. *J Biomol NMR*. **75**:303–318.

Salverda MLM, De Visser JAGM, Barlow M. 2010. Natural evolution of TEM-1 β-lactamase: experimental reconstruction and clinical relevance. *FEMS Microbiol Rev*. **34**:1015–1036.

Savard P-Y, Gagné SM. 2006. Backbone dynamics of TEM-1 determined by NMR: evidence for a highly ordered protein. *Biochemistry* **45**:11414–11424.

Sekhar A, Kay LE. 2019. An NMR view of protein dynamics in health and disease. *Annu Rev Biophys*. **48**:297–319.

Shen Y, Delaglio F, Cornilescu G, Bax A. 2009. TALOS+: a hybrid method for predicting protein backbone torsion angles from NMR chemical shifts. *J Biomol NMR*. **44**:213–223.

Smock RG, Gierasch LM. 2009. Sending signals dynamically. *Science* **324**:198–203.

Tokuriki N, Tawfik DS. 2009. Protein dynamism and evolvability. *Science* **324**:203–207.

Tomatis PE, Fabiane SM, Simona F, Carloni P, Sutton BJ, Vila AJ. 2008. Adaptive protein evolution grants organismal fitness by improving catalysis and flexibility. *Proc Natl Acad Sci U S A*. **105**: 20605–20610.

Tooke CL, Hinchliffe P, Bonomo RA, Schofield CJ, Mulholland AJ, Spencer J. 2021. Natural variants modify *Klebsiella pneumoniae*

carbapenemase (KPC) acyl–enzyme conformational dynamics to extend antibiotic resistance. *J Biol Chem*. **296**:100126.

Tooke CL, Hinchliffe P, Bragginton EC, Colenso CK, Hirvonen VHA, Takebayashi Y, Spencer J. 2019. β-Lactamases and β-lactamase inhibitors in the 21st century. *J Mol Biol*. **431**:3472–3500.

Vallurupalli P, Bouvignies G, Kay LE. 2012. Studying "invisible" excited protein states in slow exchange with a major state conformation. *J Am Chem Soc*. **134**:8148–8161.

VanPelt J, Shurina BA, Ramelot TA, Bonomo RA, Page RC. 2019. (1) H, (13)C, and (15)N backbone resonance assignments for KPC-2, a class A serine-β-lactamase. *Biomol NMR Assign*. **13**: 139–142.

Vranken WF, Boucher W, Stevens TJ, Fogh RH, Pajon A, Llinas M, Ulrich EL, Markley JL, Ionides J, Laue ED. 2005. The CCPN data model for NMR spectroscopy: development of a software pipeline. *Proteins Struct Funct Bioinforma*. **59**:687–696.

Weikl TR, Paul F. 2014. Conformational selection in protein binding and function: conformational selection. *Protein Sci*. **23**:1508–1518.

Weinreich DM, Delaney NF, Depristo MA, Hartl DL. 2006. Darwinian evolution can follow only very few mutational paths to fitter proteins. *Science* **312**:111–114.

Zou T, Risso VA, Gavira JA, Sanchez-Ruiz JM, Ozkan SB. 2015. Evolution of conformational dynamics determines the conversion of a promiscuous generalist into a specialist enzyme. *Mol Biol Evol*. **32**:132–143.